Lawrence Berkeley National Laboratory
Lawrence Berkeley National Laboratory

Title

Wintertime pytoplankton bloom in the Subarctic Pacific supported by continental margin iron

Permalink

https://escholarship.org/uc/item/84f708qm

Authors

Lam, Phoebe J.
Bishop, James K.B.
Henning, Cara C.
et al.

Publication Date

2008-06-04

Peer reviewed

The continental margin as a source of iron to the open ocean

Phoebe J. Lam[1,2], James K.B. Bishop[1], Cara C. Henning[3], Matthew A. Marcus[4], Glenn A. Waychunas[1] & Inez Y. Fung[3]

[1]*Earth Sciences Division, Lawrence Berkeley National Laboratory, 1 Cyclotron Road, Berkeley, CA 94720, USA*

[2]*Department of Earth and Planetary Science, University of California, Berkeley, Berkeley, CA 94720, USA*

[3]*Berkeley Atmospheric Sciences Center, University of California, Berkeley, Berkeley, CA 94720, USA*

[4]*Advanced Light Source, Lawrence Berkeley National Laboratory, 1 Cyclotron Road, Berkeley, CA 94720, USA*

Iron is a limiting nutrient in large areas of the world oceans. The major sources of iron to the open ocean are thought to be from atmospheric dust deposition and from upwelling [1-7]. Here we present the first observation of the distribution of particulate iron within marine aggregates to support the hypothesis that the continental margins are an additional source of iron to the open oceans. Using synchrotron x-ray techniques, we find that discrete micron-sized iron-rich hotspots are prevalent in marine aggregates in the northeast Subarctic Pacific, an iron limited region. Iron hotspot concentrations ranged from 8-20 pM at Ocean Station Papa and exceeded 700 pM at the coast. The hypothesis that hotspots are evidence for a continental margin

iron source is supported by the mineral nature of the iron hotspots, an increasing concentration gradient of hotspots towards the coast, and the absence of Asian dust delivery to the area at this time. The delivery of continental margin iron to the open ocean is confirmed using an ocean general circulation model with an iron-like tracer source at the continental margin.

We collected size-fractionated (1-53 µm and >53 µm) particulate samples using the Multiple Unit Large Volume in-situ Filtration System (MULVFS)[8] from Ocean Station Papa (OSP, 50°N 145°W) in the northeast Subarctic Pacific in February 1996 and at inshore stations (P4, P16) along a coastal to open ocean transect in February 1997 (cf. Fig. 4). MULVFS samples were also collected from the Subantarctic South Pacific (55°S, 170°W) during the 2002 Southern Ocean Iron Experiment (SOFeX)[9,10].

Surprisingly, >53 µm samples obtained from the 110 m-deep winter-time mixed layer at OSP in February 1996 were dominated by large chain forming diatoms (*Fragilariopsis sp.* and *Chaetoceros sp.*) and accompanied by abundant large (hundreds of microns) aggregates loaded with coccoliths. Total particulate Si and $CaCO_3$ levels in the mixed layer in February were anomalously high (300 and 350 nM, respectively). A diatom dominated assemblage like the one observed in February 1996 at OSP is more typical of an iron replete rather than an iron limited region[11]. We therefore surmise that there was a recent source of bioavailable iron to this region in February.

We mapped the distribution of iron in a subset of >53 µm MULVFS samples from the Subarctic Pacific and from SOFeX using the synchrotron x-ray fluorescence (XRF) microprobe at beamline 10.3.2 at the Advanced Light Source (ALS), Lawrence Berkeley National Laboratory[12]. A typical 1 mm^2 XRF map represented ~1/50,000 of the entire

MULVFS filter whose size and particulate mass are known. XRF analysis of mixed layer samples collected in February 1996 at OSP showed that iron was distributed as micron-sized discrete hotspots within the aggregates (Fig. 1a). This is in stark contrast with calcium maps, which showed that micron sized coccoliths were spread evenly throughout the aggregates (Fig. 1b). Aggregates loaded with iron hotspots occurred ubiquitously in all samples studied, including our deepest sample at 900m (Fig. S1). For comparison, >53 μm samples in the Southern Ocean, far from any continental margin, showed far fewer hotspots (Fig. 1c,d).

We corrected the Fe XRF data for artifactual counts and quantified them using a Fe XRF membrane standard (Suppl.Methods). We determined the XRF detection limit (1×10^{-11} μmol Fe/μm^2) as three times the standard deviation of corrected Fe XRF counts of a blank. We defined a Fe hotspot threshold to be fifteen times the detection limit. XRF detectable and hotspot Fe were the sum of all Fe from pixels above the detection limit and hotspot threshold, respectively. XRF map Fe values were corrected for selection bias using bulk Ca and Mn determined by ICP-MS and divided by the equivalent volume filtered to convert to concentrations of iron in the water column (Suppl.Methods).

The concentration of iron hotspot particles at a depth of ~90 m was 19 pM at OSP, 37 pM at P16, and 1233 pM at P4 near the coast in the Subarctic Pacific (Fig. 2), while it was only 2 pM in the Southern Ocean sample (15 m, before Fe addition). This amounted to 32% (OSP), 47% (P16), 92% (P4), and 45% (SOFeX) of XRF detectable Fe. XRF detectable Fe tended to be less than acid-leachable Fe determined by ICP-MS (Fig. 2). The difference between ICP-MS and XRF detectable Fe can be explained by a significant portion of the iron occurring below the pixel by pixel based detection limit, but the detection of hotspots is unequivocal since the hotspot threshold is significantly above the detection limit. The

prevalence of iron hotspots within aggregates also increased by orders of magnitude from OSP towards the coast, with hotspot iron concentrations at ~90 m of ~30 ppm (μmol Fe/mol Particulate Organic Carbon) at OSP, ~400 ppm at P16, and ~10,000 ppm at P4.

We have conducted preliminary analyses of the iron speciation of the hotspots using Extended X-ray Absorption Fine Structure (EXAFS) (Suppl.Methods). EXAFS data of an iron hotspot from a mixed-layer (46 m) sample from OSP was well fit with a linear combination of iron hydroxide (60% goethite) and amorphous iron oxyhydroxide (40% ferrihydrite) (Fig.S2a). The second shell of another hotspot from the same sample was best fit with Si as an electron backscatterer (Fig.S2b), implying that Fe-silicates are also a component of the hotspots.

The hotspot iron is unevenly distributed in the marine aggregate and is not correlated with Ca, suggesting that iron-rich particles may have been inadvertently incorporated into the marine aggregates or precipitated within the aggregate. Given the discrete and predominantly hydroxide nature of the iron hotspots, we examine their three possible origins: authigenic formation (*in-situ* precipitation), atmospheric dust delivery, and oceanic transport from the continental margin.

The Fe oxides could have their origin in reducing marine sediments or local authigenic precipitation. Our strongest evidence arguing against *in-situ* precipitation of the iron-rich particles comes from samples collected during SOFeX at 55°S, 170°W. A sample collected at the base of the mixed-layer inside the iron-enriched patch 3 weeks after multiple iron additions did not show evidence of additional hotspot formation (Fig. 1d), showing about the same level of hotspot Fe before and after iron addition (1 pM of hotspot Fe after compared to 2 pM before), despite a more than three-fold increase in acid-

leachable Fe from 70 pM to 256 pM. In addition, the heterogeneous speciation of the hotspots (Fig.S2; Table SM3) argues against *in-situ* precipitation.

Atmospheric dust delivery from Asia is an unlikely source of the iron because the gradient in concentration of iron-rich particles increases eastward towards the coast (Fig. 2), which is the opposite of what one would expect if the iron source was Asian dust. In addition, there is no record of any major dust events to the Subarctic Pacific prior to our sample collection (Fig.S3).

The increasing gradient of iron-rich particles towards the Canadian coast suggests that the source of the iron-rich particles is from the continental margin. Profiles of acid leachable particulate Fe and Mn show a clear concentration maximum at the depth of the continental margin, and hint at the offshore propagation of this signal (Fig. 3). Evidence from the California coast shows that high concentrations of dissolvable iron (up to 110 nM, similar to P4) in surface waters can be explained by the entrainment of particles from the continental shelf[13,14], and that this signal can be transported offshore[15]. The Subarctic Pacific exhibits a strong horizontal pycnocline that is present year round. This pycnocline is at about the depth of the continental margin (σ_θ=26.25 at 200 m at the coast) and may provide a ready connection from the continental shelf sediments to the open ocean. Thus, reducing conditions within continental shelf sediments result in remobilization of iron and the formation of oxyhydroxides in near bottom waters. The fine hydroxide material and resuspended silicates are transported far offshore by ocean circulation, where some fraction is captured into aggregates and are observed as iron hotspots.

To examine the plausibility of iron transport from the continental margin, we ran the ocean module of the Community Climate System Model[16] with a biologically inert tracer

whose source was a constant unit flux (1 μmol/m^2/day) from the continental margin down to 200 m (Fig. 4). We simulate the loss of this tracer from gravitational settling by assigning low and high sinking velocities (10^{-4} cm/s and 10^{-3} cm/s) to the tracers. These represent the Stokes' sinking velocities of spherical iron hydroxide-like particles with diameters of 1 and 3 μm, respectively, which are reasonable given the calculated size of our iron-rich particles (cf. Fig. 1). The model is run at relatively coarse resolution (~1° in the North Pacific), but includes parameterizations for eddy-induced mixing. After 1.5 years, the "1-μm" tracer distribution (Fig. 4) resembles that observed, in terms of both the direction and relative magnitude of the iron hotspot gradient (Fig. 2), with ~10^3 pM at OSP, ~10^4 pM at P16, and ~10^6 pM at P4. The "3-μm" tracer settles out before reaching OSP.

The large-scale cyclonic circulation in the Subarctic Pacific would tend to decrease the tracer concentration offshore. Examination of the different terms of the tracer tendency equation at P16, however, reveals that the horizontal eddy mixing term and vertical advection due to sinking tracer dominate the horizontal advection. The importance of the horizontal eddy mixing term is consistent with observations of the offshore (westward) transport of major nutrients by mesoscale eddies in the Northeast Subarctic Pacific[17]. Iron at OSP is predominantly from advective transport from the northwest, with its source at the Alaskan margin. It is important to note that this is the simplest case tracer model with only gravitational settling as a sink. It provides an upper limit estimate for the delivery of iron to OSP from the continental margin and confirms the possibility of the oceanic delivery of continental margin iron to the open ocean within a reasonable time scale.

The bioavailability of the Fe hotspots themselves is unanswered, but the unusual phytoplankton assemblage in February in the North Pacific indicates that the transport of mineral iron from the continental shelf is accompanied by a supply of bioavailable iron,

demonstrating that iron from the continental margins is an important and previously ignored source to the open oceans. The Subarctic Pacific is thought to be one of the three major iron limited regions of the oceans[18]. Together with recent observations of biomass stimulation by Asian dust inputs[19], our observations imply that iron limitation in the Subarctic Pacific is often relieved by natural sources.

1.   Fung, I. Y. et al. Iron supply and demand in the upper ocean. *Global Biogeochemical Cycles* **14**, 281-295 (2000).

2.   Archer, D. E. & Johnson, K. A Model of the iron cycle in the ocean. *Global Biogeochemical Cycles* **14**, 269-279 (2000).

3.   Lefevre, N. & Watson, A. J. Modeling the geochemical cycle of iron in the oceans and its impact on atmospheric CO2 concentrations. *Global Biogeochemical Cycles* **13**, 727-736 (1999).

4.   Parekh, P., Follows, M. J. & Boyle, E. Modeling the global ocean iron cycle. *Global Biogeochemical Cycles* **18** (2004).

5.   Landing, W. M. & Bruland, K. W. The Contrasting Biogeochemistry of Iron and Manganese in the Pacific-Ocean. *Geochimica Et Cosmochimica Acta* **51**, 29-43 (1987).

6.   Martin, J. H., Gordon, R. M. & Fitzwater, S. E. The Case for Iron. *Limnology and Oceanography* **36**, 1793-1802 (1991).

7.   Johnson, K. S., Gordon, R. M. & Coale, K. H. What controls dissolved iron concentrations in the world ocean? *Marine Chemistry* **57**, 137-161 (1997).

8.   Bishop, J. K. B., Schupack, D., Sherrell, R. M. & Conte, M. A Multiple-Unit Large-Volume In-situ Filtration System for Sampling Oceanic Particulate Matter in Mesoscale Environments. *Advances in Chemistry Series*, 155-175 (1985).

9.   Coale, K. H. et al. Southern ocean iron enrichment experiment: Carbon cycling in high- and low-Si waters. *Science* **304**, 408-414 (2004).

10.   Bishop, J. K. B., Wood, T. J., Davis, R. E. & Sherman, J. T. Robotic observations of enhanced carbon biomass and export at 55 degrees S during SOFeX. *Science* **304**, 417-420 (2004).

11.   Price, N. M., Ahner, B. A. & Morel, F. M. M. The Equatorial Pacific-Ocean - Grazer-Controlled Phytoplankton Populations in an Iron-Limited Ecosystem. *Limnology and Oceanography* **39**, 520-534 (1994).

12.   Marcus, M. A. et al. Beamline 10.3.2 at ALS: a hard X-ray microprobe for environmental and materials sciences. *Journal of Synchrotron Radiation* **11**, 239-247 (2004).

13.   Fitzwater, S. E. et al. Iron, nutrient and phytoplankton biomass relationships in upwelled waters of the California coastal system. *Continental Shelf Research* **23**, 1523-1544 (2003).

14.   Johnson, K. S., Chavez, F. P. & Friederich, G. E. Continental-shelf sediment as a primary source of iron for coastal phytoplankton. *Nature* **398**, 697-700 (1999).

15.   Johnson, K. S. et al. Surface ocean-lower atmosphere interactions in the Northeast Pacific Ocean Gyre: Aerosols, iron, and the ecosystem response. *Global Biogeochemical Cycles* **17** (2003).

16.   Blackmon, M. et al. The Community Climate System Model. *Bulletin of the American Meteorological Society* **82**, 2357-2376 (2001).

17.   Whitney, F. & Robert, M. Structure of Haida eddies and their transport of nutrient from coastal margins into the NE Pacific Ocean. *Journal of Oceanography* **58**, 715-723 (2002).

18.   Boyd, P. W. et al. The decline and fate of an iron-induced subarctic phytoplankton bloom. *Nature* **428**, 549-553 (2004).

19.   Bishop, J. K. B., Davis, R. E. & Sherman, J. T. Robotic observations of dust storm enhancement of carbon biomass in the North Pacific. *Science* **298**, 817-821 (2002).

Supplementary Information accompanies the paper on *Nature*'s website (http://www.nature.com).

Competing Interests. The authors declare they have no competing financial interests.

Correspondence and requests for materials should be addressed to P.J.L. (e-mail: pjlam@socrates.berkeley.edu).

Figure 1. X-Ray Fluorescence (XRF) maps of marine aggregates. **a.** FeKα map of an Ocean Station Papa (OSP) sample from 71 m showing Fe hotspot distribution; **b.** CaKα map of same sample showing aggregate locations; two foraminifera visible; **c.** FeKα map of a Southern Ocean sample collected from 15 m at 55°S, 170°W during SOFeX before Fe addition, showing few Fe hotspots; and **d.** FeKα

map of a sample from SOFeX from 35 m, three weeks after multiple iron additions, also showing few Fe hotspots. Acid-leachable Fe determined (overnight leach in 0.6 N HCl at 60°C) by ICP-MS was of the same order of magnitude for the OSP (103 pM) and SOFeX (-Fe: 70 pM; +Fe: 256 pM) samples, arguing against authigenic precipitation of Fe within the aggregates. CaKα XRF was used to locate aggregates from OSP since they were loaded with $CaCO_3$ coccoliths. FeKα XRF counts were corrected for artifactual counts (Suppl.Methods). Colour bars are in μmol (Fe or Ca) x 10^9/pixel, and are limited to a fixed range for comparison. Maximum and minimum values of each map are indicated. The pixel size was 5 μm. Assuming a hotspot was a single iron-rich particle, we calculated a typical Fe hotspot (9 x 10^{-9} μmol Fe) with an iron hydroxide (FeOOH, density=3.8 g/cm^3) or generic Fe-silicate (5% Fe, density=3 g/cm^3) composition to have diameters of 0.7 μm and 1.9 μm, respectively.

Figure 2. Increasing gradient in concentration of Fe hotspots (diamonds), XRF-detectable Fe (circles), and acid-leachable Fe (triangles) from the open ocean to the coast. The gradient is suggestive of a continental source. Fe hotspots are plotted against actual distance of stations from shore; XRF-detectable and acid leachable Fe are offset by -25 and -50 km, respectively, for clarity. Only >53μm samples from the upper 200 m are plotted. XRF-detectable Fe was roughly 50% of acid leachable Fe determined by ICP-MS. Stations are OSP, P16, and P4 from left to right. OSP samples were collected in February 1996; P16 and P4 samples were collected in February 1997.

Figure 3. Acid leachable particulate Fe and Mn profiles at OSP (diamonds), P16 (right triangles), and P4 (left triangles). Fe and Mn distributions are dominated by

fine particles, and have concentration maxima at the depth of the continental margin (150-200 m). The pycnocline is nearly horizontal in the Subarctic Pacific, facilitating the offshore transport of fine particles from the continental shelf. 1-53 μm Fe (top) and Mn (bottom) plotted as filled symbols. >1 μm Fe and Mn plotted as open symbols.

Figure 4. Iron-like tracer concentrations in Subarctic Pacific from an ocean general circulation model. Station locations, shown as black X's, are OSP, P16, and P4 from left to right. Tracer source regions are shown as white dots. The model was run for 1.5 years and shows that iron at OSP is from the Alaskan shelf, whereas iron at P16 and P4 is from the Canadian shelf. The tracer had a sinking velocity of 10^{-4} cm/s. Concentrations are in pM (log units), assuming a 1 μmol/m^2/day source flux.
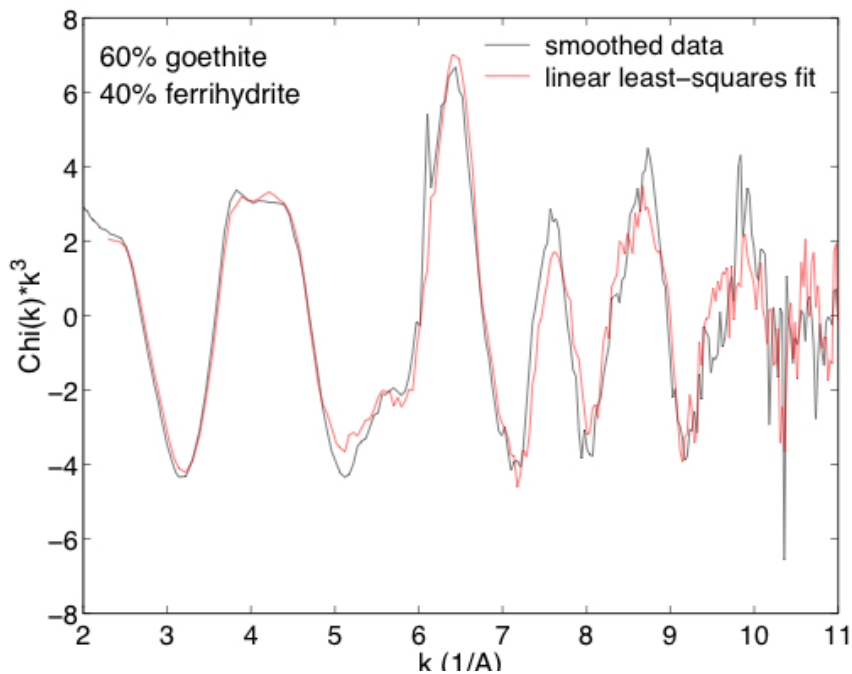
Figure S2a. EXAFS data (black) and least squares fit (red) of an iron hotspot. The EXAFS region of an iron hotspot from a 46m OSP sample from February was k^3-weighted. EXAFS spectra of model iron oxide compounds were used to fit the data. The data were fit with a linear combination of goethite (60%) and ferrihydrite (40%).
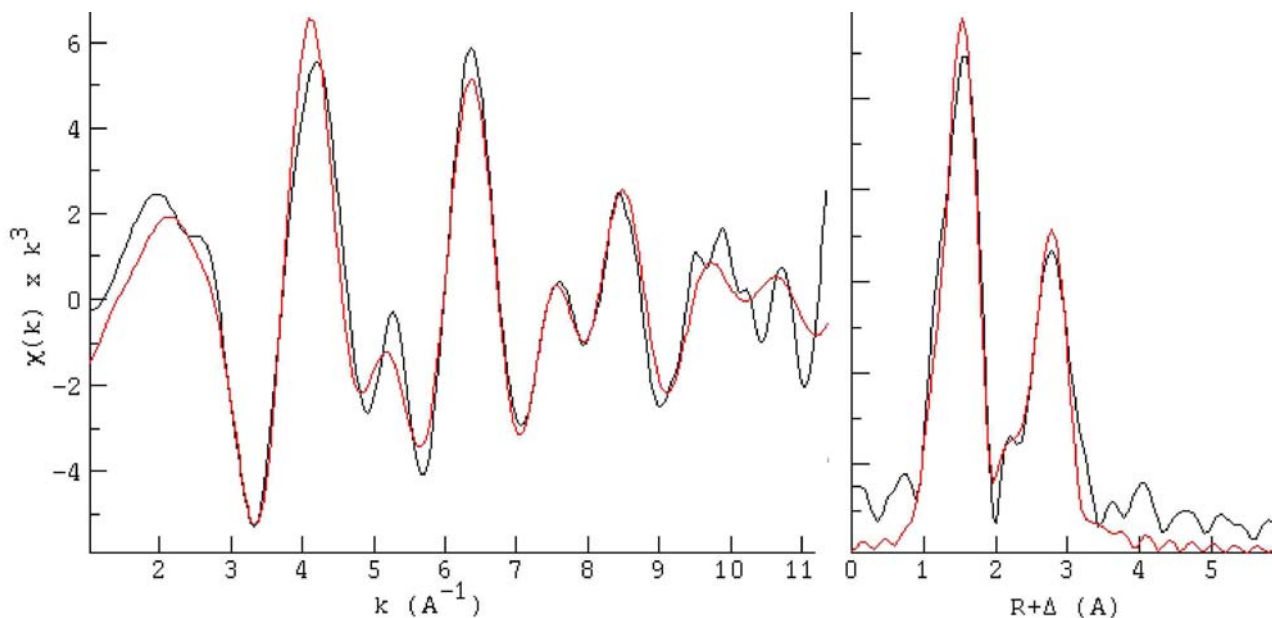

Figure S2b. EXAFS (left) and Fourier transform of EXAFS region (right) of another iron hotspot. Smoothed data in black; fit in red was for an oxygen 1st shell at 2.001 Å with a coordination number (CN) of 3.9, σ^2=0.0098, and ΔE_0=3.0 eV, and a silicon 2nd shell at 3.195 Å, with a CN of 5.7, σ^2=0.0098, and ΔE_0=2.7 eV . 1st and 2nd shells were filtered and fit using EXAFSpak and phase and amplitude functions for O, Fe, and Si generated using FEFF.
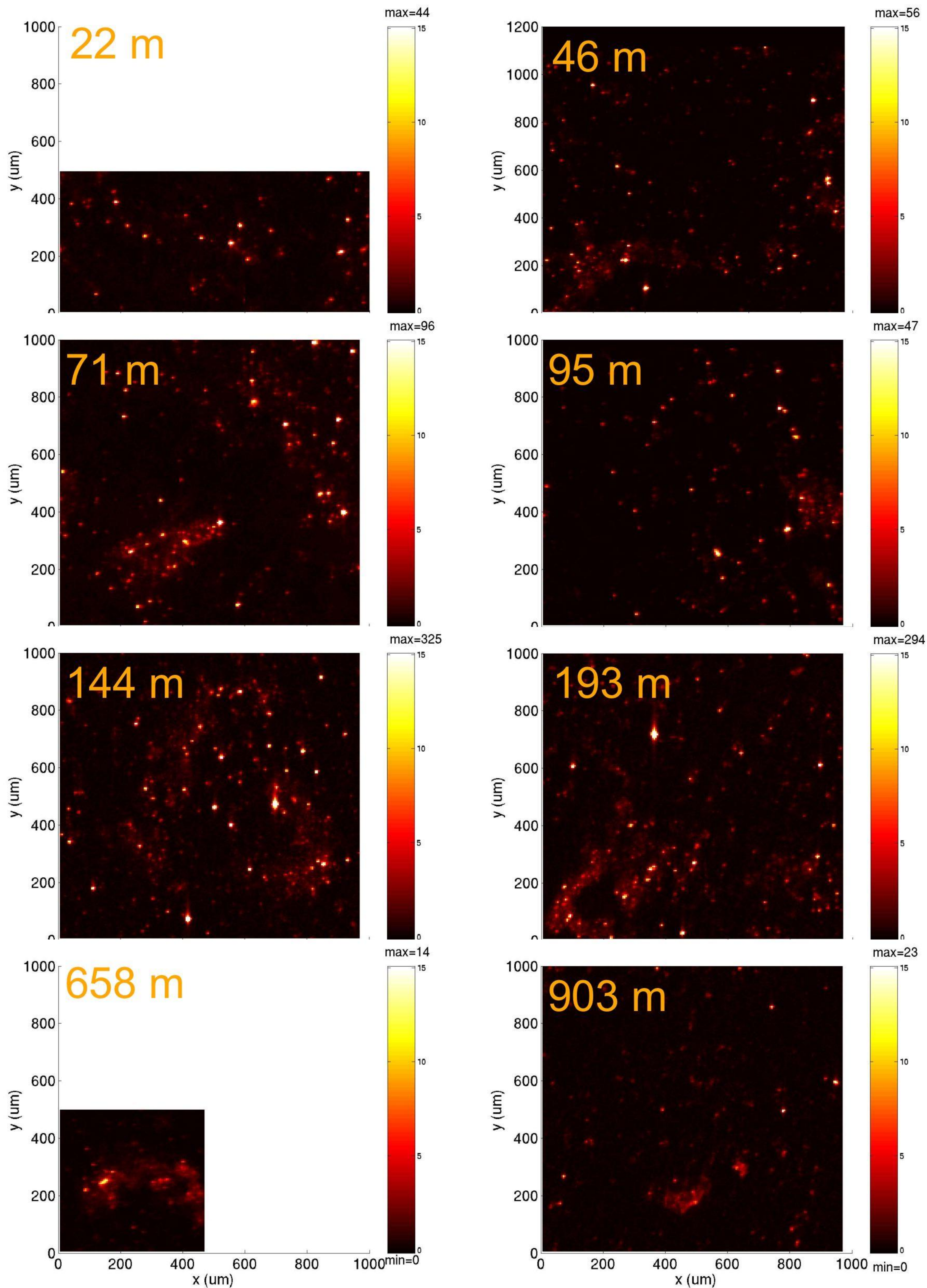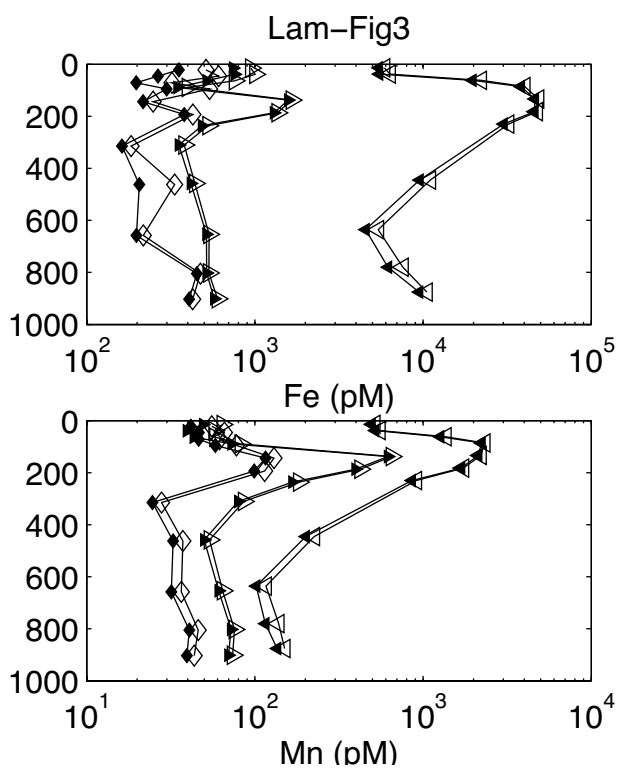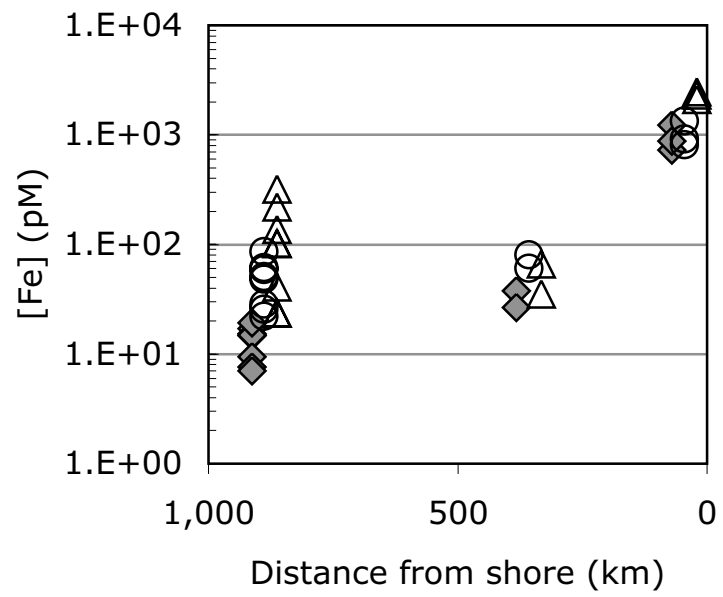
Figure S1. XRF maps of corrected Fe for samples from OSP. The x and y scales for each map are 1,000 μm. Colour bars are in μmol Fe x 10^9/pixel and are forced to a fixed range for comparison; maximum and minimum values of each map are indicated.
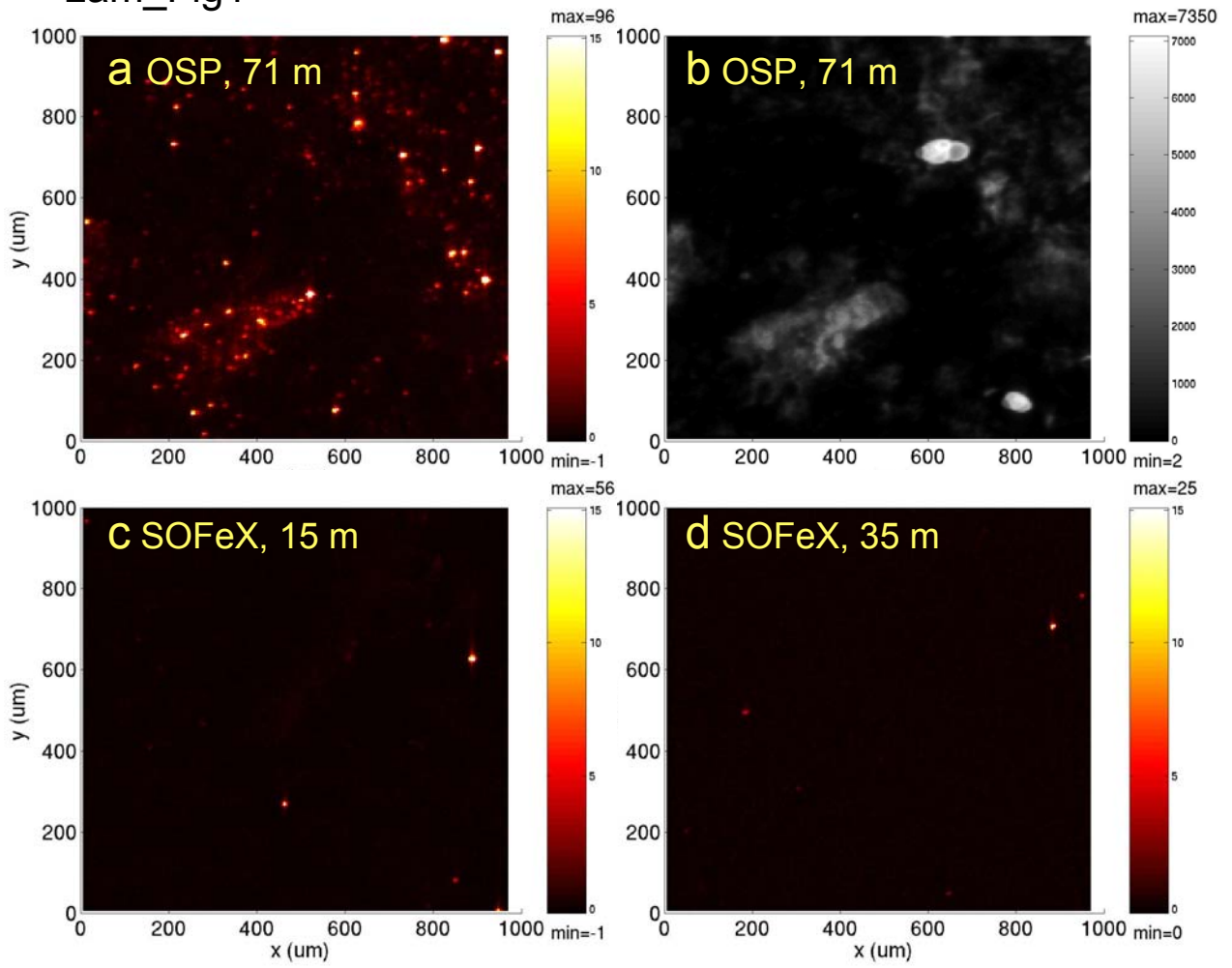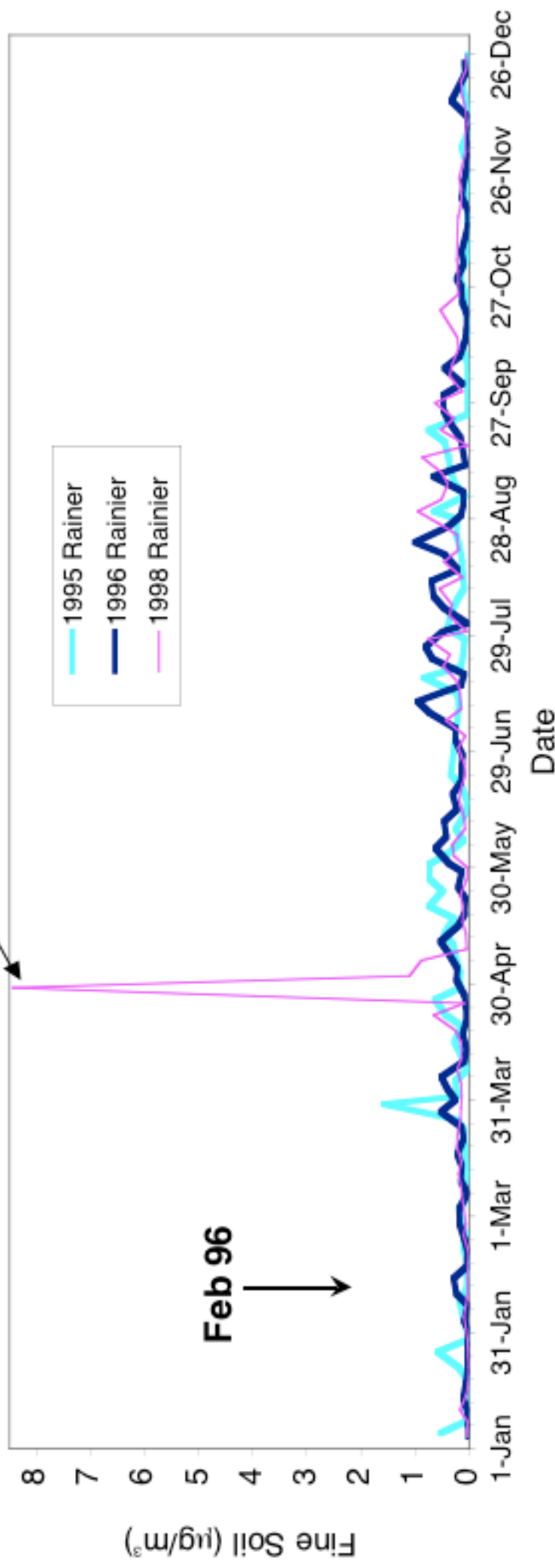
Lam–Fig3

Lam_Fig2

Lam_Fig1

Figure S3. Mineral dust recorded at Mt. Rainier National Park. Data for 1995 (light blue) and 1996 (dark blue) do not show any record of major dust events prior to sample collection in February 1996. For comparison, the Asian Dust Event of 1998[1] is clearly seen in the 1998 time series (pink). Data are from the Interagency Program for Visual Environments (IMPROVE).

1. Husar, R. B. et al. Asian dust events of April 1998. *Journal of Geophysical Research-Atmospheres* **106**, 18317-18330 (2001).